A two-scale approach for propagating cracks in a fluid-saturated porous material

A two-scale approach for propagating cracks in a fluid-saturated porous material

2010 IOP Conf. Ser.: Mater. Sci. Eng. 10 012044

(http://iopscience.iop.org/1757-899X/10/1/012044)

IOP Conf. Series: Materials Science and Engineering **10** (2010) 012044 doi:10.1088/1757-899X/10/1/012044

A two-scale approach for propagating cracks in a fluid-saturated porous material

F. Irzal[1], J. J. C. Remmers[1], J. M. Huyghe[2], R. de Borst[1], and K. Ito[2]

[1] Mechanical Engineering Department, Technical University of Eindhoven, PO Box 513, 5600 MB, Eindhoven, The Netherlands

[2] Biomedical Engineering Department, Technical University of Eindhoven, PO Box 513, 5600 MB, Eindhoven, The Netherlands

E-mail: f.irzal@tue.nl

Abstract. An extension to a finite strain framework of a two-scale numerical model for propagating crack in porous material is proposed to model the fracture in intervertebral discs. In the model, a crack is described as a propagating cohesive zone by exploiting the partition-of-unity property of finite element shape functions. At the micro-scale, the flow in the cohesive crack is modelled as viscous fluid using Stokes' equations which are averaged over the cross section of the cavity. At the macro-scale, identities are derived to couple the local momentum and the mass balance to the governing equations for a saturated porous material. The resulting discrete equations are nonlinear due to the cohesive constitutive equations and the geometrically nonlinear kinematic relations. A Newton-Raphson iterative procedure is used to consistently linearise the derived system while a Crank-Nicholson scheme takes care of the time integration of the system. The derived model is used to analyse a quasi-static crack growth in confined compression under tensile loading.

1. Introduction

Since the work of Terzaghi [1] and Biot [2], the flow in deforming porous material has received considerable attention. The subject is indeed crucial for understanding and predicting the physical behaviour of many systems of interest. Initially, the research focused on the field of petroleum and geotechnical engineering. Recently, the developed techniques have also been applied to the field of biology and medical science. Several studies have been performed in order to understand the complexity of the structure as well as the physical processes in human soft tissues, e.g. blood perfusion [3], skin and subcutis [4] and cartilaginous tissues including intervertebral discs [5]. Understanding the mechanism of soft tissues can give a huge benefit for preventing related diseases as well as for designing effective medical treatment.

This research focuses on the fracture that may occur in intervertebral discs. The intervertebral disc, which lies between adjacent vertebrae in the spine, serves as a shock absorber, load distributor, spacer and provides flexibility to the spine. The presence of damage in the discs, e.g. cracks, faults and shear bands, can obviously change the physical behaviour of the discs and affects their capacity of absorbing and transmitting load, which may result in severe lower back pains. The main goal of this research is to develop a numerical tool in order to understand the causes of this damage to reduce the medical costs associated with treating this disease.

Recently, a two-scale numerical model has been constructed for crack propagation in deforming fluid-saturated porous material subject to small strains [6, 7]. The saturated porous material is modelled as a two-phase mixture composed by the deforming solid skeleton and the interstitial fluid. The model also exploits the partition-of-unity property of finite element shape functions [8] in order to capture the nucleation and propagation of cracks independently from the underlying discretisation. At the fine scale of this model the flow in the crack is modelled as a viscous fluid using Stokes' equations. Since the cross-sectional dimensions of the cavity formed by the crack assumed to be small compared to its length, the flow equations can be averaged over the cross section of the cavity. The resulting equations provide the momentum and mass couplings with the standards equations for a porous material which hold on the coarse scale.

In this contribution, we will extend the aforementioned model to a finite strain framework. Since the soft tissues are in general subject to large deformations and mechanical loads, the model is extended by introducing nonlinear kinematics of the deformation in combination with a hyperelastic material response. The finite element equations are derived for this model and calculated in a total Lagrangian formulation. The resulting system of equations are nonlinear due to the cohesive crack model, the geometrical nonlinear effect and nonlinearity of the coupling terms. A Newton-Raphson iterative procedure is used to consistently linearise the derived system whereas a Crank-Nicholson scheme is applied to discretise the system in the time domain.

2. Governing equation for the bulk

The bulk part of the disc is considered as an incompressible two-phase porous material. Furthermore, we assume that there is no mass transfer between the constituents, the inertia effects and gravity can be neglected and the process is considered as isothermal. With these assumptions we write the balances of linear momentum for the solid and the fluid phases as follows:

$$\nabla \cdot \boldsymbol{\sigma}_\alpha + \boldsymbol{\pi}_\alpha = \mathbf{0}, \tag{1}$$

where $\boldsymbol{\sigma}_\alpha$ and $\boldsymbol{\pi}_\alpha$ denote the stress tensor of constituent α and the momentum interaction between different constituent, respectively. In the remainder of this paper we follow $\alpha = \mathrm{s}, \mathrm{f}$, with s and f denoting the solid and fluid phases, respectively. By assuming that there exists no momentum interaction between solid and summing equation 1 for solid and fluid part of the mixture, the local momentum balance of the mixture as a whole can be formulated as

$$\nabla \cdot \boldsymbol{\sigma} = \mathbf{0}, \tag{2}$$

where the stress is composed of a solid and a fluid part, $\boldsymbol{\sigma} = \boldsymbol{\sigma}_\mathrm{s} + \boldsymbol{\sigma}_\mathrm{f}$. Furthermore, under the same assumptions, the local mass balance of the constituent α reads

$$\frac{\partial \rho_\alpha}{\partial t} + \rho_\alpha \nabla \cdot \mathbf{v}_\alpha = 0, \tag{3}$$

where ρ_α denotes the apparent mass density and $\mathbf{v}_\alpha$ is the absolute velocity of constituent α. We multiply the mass balance for each constituent α by its volume fraction n_α and add them. By utilizing the constraint $\sum_{\alpha=\mathrm{s,f}} n_\alpha = 1$ and considering the incompressibility of the porous material, the local mass balance reads

$$\nabla \cdot \mathbf{v}_\mathrm{s} + \nabla \cdot (n_\mathrm{f}(\mathbf{v}_\mathrm{f} - \mathbf{v}_\mathrm{s})) = 0. \tag{4}$$

The constitutive behaviour of the mixture can be derived by applying the first law of thermodynamics and conservation of energy of each constituent to the entropy inequality of the mixture [9]. By choosing the Green-Lagrange strain tensor $\mathbf{E}$, the Lagrangian form of the fluid volume fraction Jn_f, and the relative velocity as independent variables in the description of

the mixture's constitutive behaviour, we obtain the effective stress and the constitutive relations for the relative volumetric flux of the fluid:

$$\sigma_{\mathrm{e}} = \frac{1}{J}\mathbf{F}\cdot\frac{\partial \mathbf{W}}{\partial \mathbf{E}}\cdot\mathbf{F}^{T} \tag{5}$$

$$n_{\mathrm{f}}\cdot(\mathbf{v}_{\mathrm{f}}-\mathbf{v}_{\mathrm{s}}) = -k_{\mathrm{f}}\,\mathbf{F}^{-T}\cdot\nabla_0\, p, \tag{6}$$

where $\mathbf{F}$ describes the deformation gradient, $J=\det(\mathbf{F})$ represents the relative volume change, $\mathbf{W}$ is the strain energy function of the mixture and k_{f} describes the permeability coefficient. Equation 6 is known as Darcy's equation [2], where p describes the hydrostatic pressure of the fluid. Furthermore, the effective stress $\boldsymbol{\sigma}_{\mathrm{e}}$ is defined as the deformation dependent part of the total stress in the mixture and related to the hydraulic pressure p by the relationship

$$\boldsymbol{\sigma}_{\mathrm{e}} = \boldsymbol{\sigma} + p\,\mathbf{I}, \tag{7}$$

where $\mathbf{I}$ is the identity tensor. The balance of momentum of the saturated medium, equation 2 is complemented by the boundary conditions

$$\mathbf{n}_{\Gamma}\cdot\boldsymbol{\sigma} = \bar{\mathbf{t}}, \qquad \mathbf{v} = \bar{\mathbf{v}}, \tag{8}$$

hold on complementary parts of the boundary Γ_t and Γ_v, with $\Gamma=\Gamma_t\cup\Gamma_v$, $\Gamma_t\cap\Gamma_v=\emptyset$, $\bar{\mathbf{t}}$ and $\bar{\mathbf{v}}$ are the prescribed external traction and the prescribed velocity, respectively. The balance of mass, equation 4, is complemented by the boundary conditions

$$n_{\mathrm{f}}(\mathbf{v}_{\mathrm{f}}-\mathbf{v}_{\mathrm{s}}) = \bar{\mathbf{q}}, \qquad p=\bar{p}, \tag{9}$$

hold on complementary parts of the boundary Γ_q and Γ_p, with $\Gamma=\Gamma_q\cup\Gamma_p$, $\Gamma_q\cap\Gamma_p=\emptyset$, $\bar{\mathbf{q}}$ and $\bar{p}$ being the prescribed outflow of pore fluid and the prescribed pressure, respectively. Figure 1 shows a body Ω crossed by a material discontinuity with the aforementioned boundary conditions.

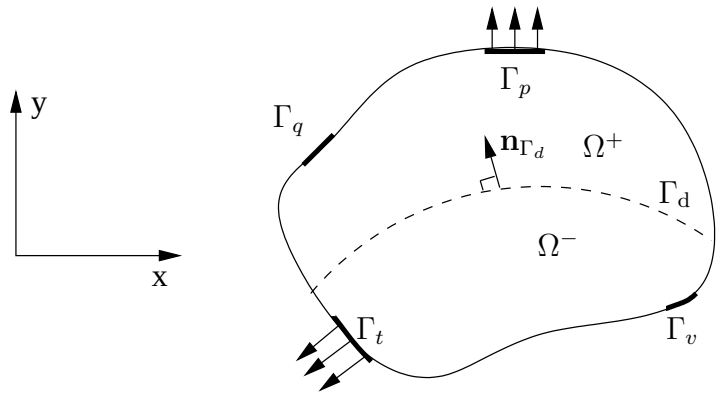

Figure 1. Body Ω crossed by a discontinuity Γ_{d} and complemented by boundary conditions. The x-y coordinate represents the global coordinate of the body.

3. Nonlinear kinematics formulation at discontinuities

Figure 2(a) shows a body crossed by a discontinuity $\Gamma_{\mathrm{d},0}$ in the reference (undeformed) configuration. The body is divided by the discontinuity into two sub-domains, Ω_0^+ and Ω_0^- ($\Omega_0=\Omega_0^+\cup\Omega_0^-$). A vector $\mathbf{n}_0$ is defined normal to the discontinuity surface $\Gamma_{\mathrm{d},0}$ in the direction

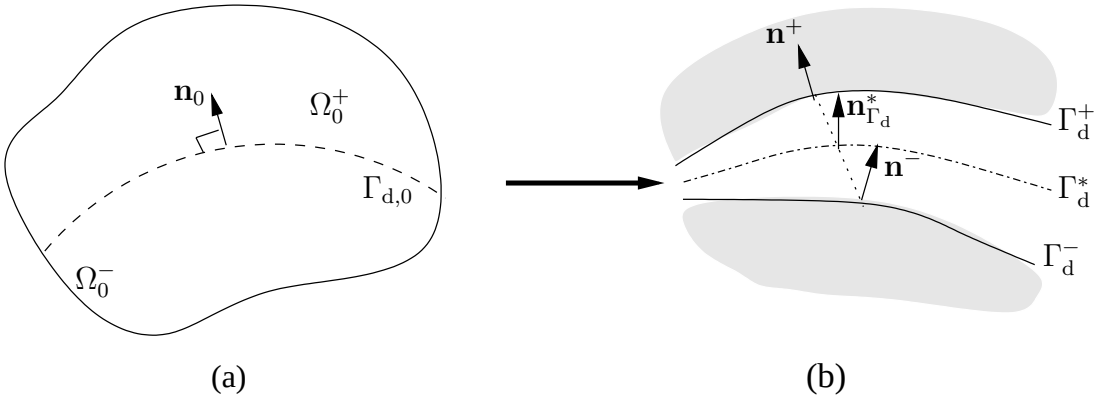

Figure 2. (a). Schematic representation of body Ω_0 crossed by a material discontinuity $\Gamma_{\mathrm{d},0}$ in the undeformed configuration. (b). Discontinuity interfaces Γ_d^+ and Γ_d^- and their normal vector representation in the deformed configuration

of Ω_0^+. The total displacement field $\mathbf{u}$ consists of a continuous regular displacement field $\hat{\mathbf{u}}$ and a continuous additional displacement field $\tilde{\mathbf{u}}$ [12]:

$$\mathbf{u} = \hat{\mathbf{u}} + \mathcal{H}_{\Gamma_{\mathrm{d},0}}\tilde{\mathbf{u}}, \tag{10}$$

where $\mathcal{H}_{\Gamma_{\mathrm{d},0}}$ is the Heaviside step function centered at the discontinuity and is defined as:

$$\mathcal{H}_{\Gamma_{\mathrm{d},0}}(\mathbf{X}) = \begin{cases} 1 & \text{if} \quad \mathbf{X} \in \Omega_0^+ \\ 0 & \text{if} \quad \mathbf{X} \in \Omega_0^-. \end{cases} \tag{11}$$

From the displacement decomposition in Equation 10, the deformation map $\Phi(\mathbf{X}, t)$ for a body crossed by a discontinuity can be written as

$$\Phi(\mathbf{X}, t) := \mathbf{x}(\mathbf{X}, t) = \mathbf{X} + \hat{\mathbf{u}}(\mathbf{X}, t) + \mathcal{H}_{\Gamma_{\mathrm{d},0}}(\mathbf{X})\tilde{\mathbf{u}}(\mathbf{X}, t), \tag{12}$$

where $\mathbf{x}$ is the position vectors of a material point in the deformed configuration. The deformation gradient is obtained by taking the gradient of equation 12 with respect to the reference configuration:

$$\mathbf{F} = \hat{\mathbf{F}} + \mathcal{H}_{\Gamma_{\mathrm{d},0}}\tilde{\mathbf{F}} + \delta_{\Gamma_{\mathrm{d},0}}(\tilde{\mathbf{u}} \otimes \mathbf{n}_{\Gamma_{\mathrm{d},0}}), \tag{13}$$

with $\hat{\mathbf{F}} = \mathbf{I} + \nabla_0\hat{\mathbf{u}}$, $\tilde{\mathbf{F}} = \nabla_0\tilde{\mathbf{u}}$, and $\delta_{\Gamma_{\mathrm{d},0}}$ the Dirac function at the interface in the reference configuration.

The magnitude of the displacement jump $\mathbf{u}_\mathrm{d}$ at the discontinuity $\Gamma_{\mathrm{d},0}$ is represented as the magnitude of the additional displacement field $\tilde{\mathbf{u}}$;

$$\mathbf{u}_\mathrm{d}(\mathbf{X}, t) = \tilde{\mathbf{u}}(\mathbf{X}, t), \qquad \mathbf{X} \in \Gamma_{\mathrm{d},0}. \tag{14}$$

With aid of Nanson's relation for the normal $\mathbf{n}$ to a surface Γ

$$\mathbf{n} = J\,\mathbf{F}^{-T}\mathbf{n}_0\frac{\mathrm{d}\Gamma_0}{\mathrm{d}\Gamma}, \tag{15}$$

the expressions for the normals at the Ω_0^- side and at the Ω_0^+ side of the interface can be derived as

$$\mathbf{n}^- = \det(\hat{\mathbf{F}})\,\hat{\mathbf{F}}^{-T}\mathbf{n}_0\frac{\mathrm{d}\Gamma_{\mathrm{d},0}}{\mathrm{d}\Gamma_\mathrm{d}^-}, \qquad \mathbf{X} \in \Omega_0^- \tag{16}$$

$$\mathbf{n}^+ = \det(\hat{\mathbf{F}} + \tilde{\mathbf{F}})\,\left(\hat{\mathbf{F}} + \tilde{\mathbf{F}}\right)^{-T}\mathbf{n}_0\frac{\mathrm{d}\Gamma_{\mathrm{d},0}}{\mathrm{d}\Gamma_\mathrm{d}^+}, \quad \mathbf{X} \in \Omega_0^+. \tag{17}$$

Figure 2(b) illustrates the normal vector at the discontinuities. Considering the fact that the magnitude of the opening $\mathbf{u}_{\mathrm{d}}$ will be relatively small, we assume that an average normal can be defined for use within the cohesive-zone model [11]:

$$\mathbf{n}^*_{\Gamma_{\mathrm{d}}} = \det\left(\hat{\mathbf{F}} + \frac{1}{2}\tilde{\mathbf{F}}\right)\left(\left(\hat{\mathbf{F}} + \frac{1}{2}\tilde{\mathbf{F}}\right)\right)^{-1}\mathbf{n}_0\frac{\mathrm{d}\Gamma_{\mathrm{d},0}}{\mathrm{d}\Gamma^*_d}. \tag{18}$$

The vector $\mathbf{n}^*_{\Gamma_{\mathrm{d}}}$ is used to define the traction vector at a discontinuity and to resolve a displacement jump into normal and tangential components.

With respect to the pressure field p we note that the pressure field is weakly discontinuous. Since the fluid velocity is related to the pressure gradient via Darcy's law, the gradient of the pressure normal to the discontinuity is therefore discontinuous across the cavity. Accordingly, the enrichment of the interpolation of the pressure must be such that the pressure itself is continuous, but has a discontinuous spatial derivative. Here, the distance function $\mathcal{D}_{\Gamma_{\mathrm{d},0}}$, defined as

$$\mathbf{n}_{\Gamma_{\mathrm{d}}} \cdot \nabla_0 \mathcal{D}_{\Gamma_{\mathrm{d},0}} = \mathcal{H}_{\Gamma_{\mathrm{d},0}} \tag{19}$$

satisfies this requirement. Accordingly, the pressure is decomposed as the regular continuous pressure field $\hat{p}$ and additional continuous pressure field $\tilde{p}$;

$$p = \hat{p} + \mathcal{D}_{\Gamma_{\mathrm{d},0}}\tilde{p}. \tag{20}$$

4. Weak formulation and the coupling

The weak equilibrium equation for momentum balance and mass balance in the reference configuration is expressed as

$$\int_{\Omega_0} \nabla_0 \delta\boldsymbol{u} : \mathbf{P}\,\mathrm{d}\Omega_0 + \int_{\Gamma_{\mathrm{d},0}} [\![\delta\boldsymbol{u}\cdot\mathbf{P}]\!]\cdot\mathbf{n}_{\Gamma_{\mathrm{d}}}\,\mathrm{d}\Gamma_0 = \int_{\Gamma_0}\delta\boldsymbol{u}\cdot\mathbf{t}_0\,\mathrm{d}\Gamma_0 \tag{21}$$

and

$$-\int_{\Omega_0}\delta p(\nabla_0\cdot\mathbf{v}_{\mathrm{s}})\mathbf{F}^{-T}J\,\mathrm{d}\Omega_0 + \int_{\Omega_0} k_{\mathrm{f}}\,\nabla_0\delta p\,\nabla_0 p\,\mathrm{d}\Omega_0 + \int_{\Gamma_{\mathrm{d},0}}\mathbf{n}_{\Gamma_{\mathrm{d}}}\cdot[\![\delta p\, n_{\mathrm{f}}(\mathbf{v}_{\mathrm{f}}-\mathbf{v}_{\mathrm{s}})]\!]\,\mathrm{d}\Gamma_0 = \int_{\Gamma_0}\delta p\,\mathbf{n}_0\cdot\mathbf{q}_0\,\mathrm{d}\Gamma_0, \tag{22}$$

where $\mathbf{P}$ is the nominal stress, $\mathbf{t}_0$ and $\mathbf{q}_0$ are the nominal traction and prescribed outflow fluid acting on $\Gamma_{t,0}$ and $\Gamma_{p,0}$, respectively, and $\delta\boldsymbol{u}$ and δp are displacement and pressure variations, respectively. The term $[\![\cdot]\!]$ describes the discontinuous part of the system of equation.

Due to the presence of a discontinuity inside the domain Ω_0, the power of the external tractions on $\Gamma_{\mathrm{d},0}$ and the normal flux through the faces of the discontinuity are essential features of the weak formulation. Indeed, these terms enable the momentum and mass couplings between the discontinuity (micro-scale) and the surrounding porous medium (macro-scale).

The momentum coupling stems from the tractions across the faces of the discontinuity and the pressure applied by the fluid in the discontinuity. Assuming the stress is continuous from the cavity to the bulk, we have

$$\mathbf{P}\cdot\mathbf{n}_{\Gamma_{\mathrm{d}}} = \mathbf{t}_{\mathrm{d}} - p\mathbf{n}_{\Gamma_{\mathrm{d}}}, \tag{23}$$

with $\mathbf{t}_{\mathrm{d}}$ the cohesive tractions. Furthermore, considering that $\mathbf{P} := \mathbf{F}\,\mathbf{S} - pJ\mathbf{F}^{-T}$, where $\mathbf{S}$ is the second Piola-Kirchhoff stress tensor, the weak form of the balance of momentum becomes

$$\int_{\Omega_0}\nabla_0\delta\boldsymbol{u} : (\mathbf{F}\,\mathbf{S} - pJ\mathbf{F}^{-T})\,\mathrm{d}\Omega_0 + \int_{\Gamma_{\mathrm{d},0}}[\![\delta\boldsymbol{u}]\!]\cdot(\mathbf{t}_{\mathrm{d}} - p\mathbf{n}_{\Gamma_{\mathrm{d}}})\mathrm{d}\Gamma_0 = \int_{\Gamma_0}\delta\boldsymbol{u}\cdot\mathbf{t}_0\,\mathrm{d}\Gamma_0. \tag{24}$$

Since the tractions have a unique value across the discontinuity, the pressure p must have the same value at both faces of the discontinuity, and consequently, this must also hold for the test function for the pressure, δp. Accordingly, the mass transfer coupling term for the fluid can be written as

$$-\int_{\Omega_0} \delta p(\nabla_0 \cdot \mathbf{v}_\mathrm{s})\mathbf{F}^{-T}\, J\, \mathrm{d}\Omega_0 + \int_{\Omega_0} k_\mathrm{f}\, \nabla_0 \delta p\, \nabla_0 p\, \mathrm{d}\Omega_0 + \int_{\Gamma_{\mathrm{d},0}} \delta p\, \mathbf{n}_{\Gamma_\mathrm{d}} \cdot \mathbf{q}_\mathrm{d}\, \mathrm{d}\Gamma_0 = \int_{\Gamma_0} \delta p\, \mathbf{n}_0 \cdot \mathbf{q}_0\, \mathrm{d}\Gamma_0, \tag{25}$$

where $\mathbf{q}_\mathrm{d} = [\![n_\mathrm{f}(\mathbf{v}_\mathrm{f} - \mathbf{v}_\mathrm{s})]\!]$ represents the fluid flux through the faces of the discontinuity.

To quantify the influence of the micro-flow inside the discontinuity on the macro-scale, we recall the balance of mass, which, for the micro-flow in the cavity reads

$$\dot{\rho}_\mathrm{f} + \rho_\mathrm{f} \nabla \cdot \mathbf{v} = 0, \tag{26}$$

subject to the assumptions of small changes in the concentrations and hence the convective terms can be neglected. Furthermore, we assume that the first term can be neglected due to the monophasic problem in the cavity and the velocities are therefore much higher than in the porous medium. By focusing on two-dimensional configuration and taking into account the aforementioned assumptions, the mass balance inside the cavity simplifies to:

$$\frac{\partial v}{\partial \zeta} + \frac{\partial w}{\partial \eta} = 0, \tag{27}$$

with $v = \mathbf{v} \cdot \mathbf{t}_{\Gamma_\mathrm{d}}$ and $w = \mathbf{v} \cdot \mathbf{n}_{\Gamma_\mathrm{d}}$ the tangential and normal components of the fluid velocity in the discontinuity, respectively. See figure 3 for clarity. Accordingly, the difference in the fluid

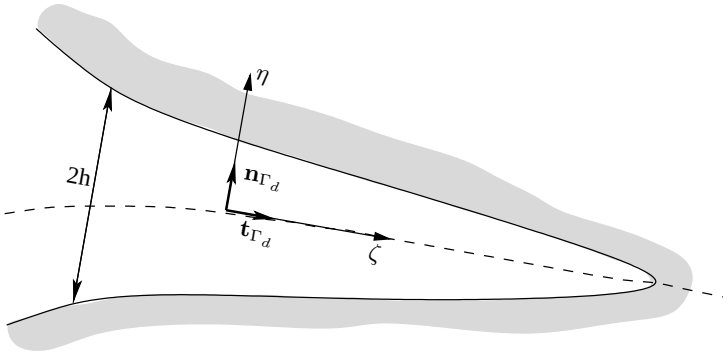

Figure 3. Geometry and local coordinate system in cavity in the deformed configuration.

velocity components that are normal to both crack faces is given by:

$$[\![w_\mathrm{f}]\!] = -\int_{-h}^{h} \frac{\partial v}{\partial \zeta} \mathrm{d}\eta. \tag{28}$$

Here, the velocity profile of the fluid flow inside the discontinuity must be known. From the balance of momentum for the fluid in the cavity and the assumption of a Newtonian fluid, the following velocity profile in the undeformed configuration results

$$v(\eta) = \frac{1}{2\mu}\mathbf{F}^{-T}\frac{\partial p}{\partial \zeta}(\eta^2 - h^2) + v_\mathrm{f}, \tag{29}$$

where an integration has been carried out from $\eta = -h$ to $\eta = h$ and μ the viscosity of the fluid. The essential boundary condition $v = v_{\mathrm{f}}$ has been applied at both faces of the cavity, and stems from the relative fluid velocity in the porous medium at $\eta = \pm h$ similar to equation 6:

$$v_{\mathrm{f}} = (\mathbf{v}_{\mathrm{s}} - \frac{k_{\mathrm{f}}}{n_{\mathrm{f}}}\mathbf{F}^{-T} \cdot \frac{\partial p}{\partial \zeta}) \cdot \mathbf{t}_{\Gamma_{\mathrm{d}}}. \tag{30}$$

Substitution of equation 29 into equation 28 and integrating with respect to η yields:

$$[\![w_{\mathrm{f}}]\!] = \frac{2}{3\mu}\mathbf{F}^{-T}\frac{\partial}{\partial \zeta}\left(\frac{\partial p}{\partial \zeta}h^3\right) - 2h\frac{\partial v_{\mathrm{f}}}{\partial \zeta} \tag{31}$$

The equation gives the amount of fluid attracted in the tangential fluid flow. It can be included in the weak form of the mass balance of the macro-flow to ensure the coupling between the micro-flow and the macro-flow. Since the difference in the normal velocity of both crack faces is given by $[\![w_{\mathrm{f}}]\!] = 2\frac{\partial h}{\partial t}$, the mass coupling term becomes

$$\begin{aligned} \mathbf{n}_{\Gamma_{\mathrm{d}}} \cdot \mathbf{q}_{\mathrm{d}} &= n_{\mathrm{f}}[\![w_{\mathrm{f}} - w_{\mathrm{s}}]\!] \\ &= n_{\mathrm{f}}\left(\frac{2h^3}{3\mu}\mathbf{F}^{-T}\frac{\partial^2 p}{\partial \zeta^2} + \frac{2h^2}{\mu}\mathbf{F}^{-T}\frac{\partial p}{\partial \zeta}\frac{\partial h}{\partial \zeta} - 2h\frac{\partial v_{\mathrm{f}}}{\partial \zeta} - 2\frac{\partial h}{\partial t}\right). \end{aligned} \tag{32}$$

5. Discretisation and linearisation of the weak equations

To cast the weak governing equation 24 in a discretised format, the functions $\mathbf{u}$, and their gradients must be expressed in terms of discrete nodal values as follows

$$\mathbf{u} = \mathbf{N}\hat{\mathbf{a}} + \mathcal{H}_{\Gamma_{\mathrm{d},0}}\mathbf{N}\tilde{\mathbf{a}}, \tag{33}$$

where $\mathbf{N}$ is a matrix containing the finite element shape functions, $\hat{\mathbf{a}}$ is 'regular' nodal degrees of freedom and $\tilde{\mathbf{a}}$ is 'additional' nodal degrees of freedom. This interpolation can be formally regarded as based on a partition of unity [10]. In the same manner, pressure field is also approximated as

$$p = \mathbf{H}\hat{\mathbf{p}} + \mathcal{D}_{\Gamma_{\mathrm{d},0}}\mathbf{H}\tilde{\mathbf{p}}, \tag{34}$$

where $\mathbf{H}$ contains the shape functions H_i used to interpolate the pressure field p and $\hat{\mathbf{p}}$ and $\tilde{\mathbf{p}}$ are the nodal arrays assembling the amplitudes that correspond to the regular and enhanced pressure field, respectively.

The choice for N_i and H_i is driven by modelling requirements. Indeed, the modelling of the fluid flow inside the cavity needs the second derivative of the pressure as seen in equation 32. Hence, the order of the finite element shape function H_i has to be sufficiently high, otherwise the coupling between the fluid flow in the cavity and the bulk part will not be achieved. Furthermore, the order of the finite element shape function N_i must be greater than or equal to the order of H_i for consistency in the discrete balance of momentum. However, in practice we will use higher order elements with quadrilateral shape functions for the displacement as well as for the pressure discretisation.

Since a Bubnov-Galerkin formulation is followed, variations of displacement and pressure are interpolated in the same manner. Hence, inserting the discretised variations of displacements and pressures into the weak forms as described in equation 24 and equation 25 yields the discretised version of the equilibrium equations for all admissible variations of displacement and pressure. The resulting discretised equations are nonlinear due to cohesive constitutive equations and geometrically nonlinear kinematic relations. Here we use Newton-Raphson method to consistently linearise the system of equations.

To carry out time integration in the resulting system a Crank-Nicholson scheme is adopted

$$\begin{aligned}\left(\frac{\partial(\cdot)}{\partial t}\right) &= \frac{(\cdot)^{t+\Delta t}-(\cdot)^{t}}{\Delta t}\\ (\cdot) &= \theta(\cdot)^{t+\Delta t}+(1-\theta)(\cdot)^{t}\end{aligned} \tag{35}$$

where Δt is the time increment, while $(\cdot)^t$ and $(\cdot)^{t+\Delta t}$ denote the unknowns displacement field $\mathbf{u}$ or pressure field p at t and $t+\Delta t$, respectively. This means that differential terms are approximated linearly by looking at the difference between the current and the previous time step, and the values of the independent variables are weighted results of the current and the previous time step. Stabilized solution is reached if implicit time stepping is used, i.e. as $\theta \geq 0.5$. Taking $\theta = 1$ reduces the method to a backward finite difference.

6. Finite Element Implementation

The finite element implementation of the proposed model follows largely that presented in reference [7]. For completeness, some details of the implementation are reviewed, particularly to the resulting stiffness matrix of the system which consist of material part, geometric part and the coupling terms.

The key step in the finite element implementation is the selection of nodes to which extra enhanced degree of freedom should be added. Consider the specimen with a static interface as shown in figure 4. In the finite element model, the interface is modelled as a discontinuity in

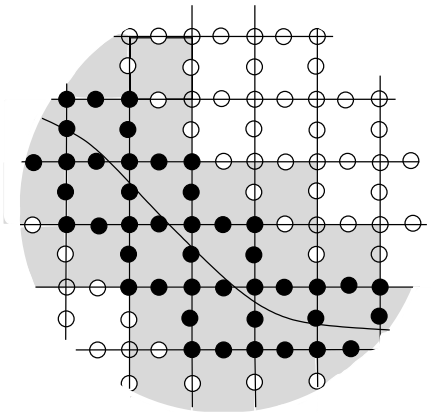

Figure 4. Two-dimensional finite element mesh with a discontinuity denoted by the bold line. Nodes with enhanced degrees of freedom are indicated by solid dots. The grey elements contain additional terms in the stiffness matrix and the internal force vector.

a structured mesh composed of eight node elements. Over the support of a node away from a discontinuity, the Heaviside function is equivalent to a constant function, one on Ω^+ and zero on Ω^-. Since the standard shape function is able to reproduce a constant field, the addition of enhanced degrees of freedom to nodes whose support is not crossed by a discontinuity would lead to a system of equations which is not linearly independent. This is violation with requirement of the partition of unity method that the shape function and the enhanced base must be linear independent [10]. Therefore, additional degrees of freedom are added only to nodes whose support is crossed by a discontinuity. The other nodes remain unchanged. Since only the nodes of elements that are crossed by the discontinuity have additional degrees of freedom, the total number of degrees of freedom of the system is slightly larger than for the case without a discontinuity.

When an element is supported by one or more enriched nodes, its stiffness matrix and force vector will obtain the additional terms. The elements that contain a discontinuity as well, will be augmented with the surface integrals that govern the cohesive behaviour. The additional terms, i.e, the cohesive traction of equation 23, the coupling terms from equation 32 and the terms in the geometric stiffness matrix due to the interface cause the resulting stiffness matrix to become asymmetry. To restore the symmetry, the contributions due to coupling terms are omitted.

This restoration of symmetry will only slightly decrease the convergence rate as this leads to a modified Newton-Raphson algorithm [11]. Nevertheless, the symmetric format of the stiffness matrix allows for more flexibility in the implementation as well as a better conditioning of the matrix.

7. Conclusions

An endeavour has been made to extend the existing two-scale model of propagating cracks in porous material into a finite strain framework. The crack which is described as a propagating cohesive zone can be located arbitrarily, independent from the underlying discretisation of the material structure. A two-scale approach has been chosen to model the fluid flow in the fractured porous material, where the fluid flow inside the cracks is modelled independently from the fluid flow in the surrounding porous material. The momentum and the mass transfer couplings between the two scales are obtained by inserting the homogenised constitutive relations of the micro-flow into the weak form of the balance equations of the bulk material under the assumption that the opening of the cohesive zone is small. The resulting formulation is implemented under finite element framework by exploiting the partition of unity property of the finite element polynomial shape functions. The performance of the proposed model remains to be demonstrated for a quasi-static crack growth in confined compression under tensile loading.

References

[1] Terzaghi K 1943 *Theoretical Soil Mechanics* (New York: Wiley)
[2] Biot M A 1941 *J. Appl. Phys.* **12** 155
[3] Vankan W J, Huyghe J M, Slaaf D W, van Donkelaar C C, Drost M, Janssen J D and Huson A 1997 *Am. J. Physiol.* **273** H1587
[4] Oomens C W J, van Campen D H and Grootenboer H J 1987 *J. Biomech.* **20** 877
[5] Malakpoor K, Kaasschieter E F and Huyghe J M 2007 *ESAIM:M2AN* **41(4)** 679
[6] Kraaijeveld F, Huyghe J M, Remmers J J C, de Borst R and Baaijens F P T (submitted) 2010 *Engng. Fracture Mech.*
[7] Rethoré J, Abellan M and de Borst R 2006 *Arch. Appl. Mech.* **75** 595
[8] Remmers J J C, de Borst R and Needleman A 2003 *Comp. Mech.* **31(1)** 69
[9] Bowen, R M 1980 *Int. J. Engng. Sci.* **18** 1129
[10] Babuska I, Melenk J M 1997 *Int. J. Numer. Meth. Engng.* **40(4)** 727
[11] Wells G N, de Borst R and Sluys L J 2002 *Int. J. Numer. Meth. Engng.* **54** 1333
[12] Wells G N and Sluys L J 2001 *Int. J. Numer. Meth. Engng.* **50(12)** 2667